Multiple fluvial processes detected by riverside seismic and infrasound monitoring of a controlled flood in the Grand Canyon

Brandon Schmandt,[1] Richard C. Aster,[2,3] Dirk Scherler,[4] Victor C. Tsai,[4,5] and Karl Karlstrom[1]

Received 28 July 2013; revised 6 September 2013; accepted 9 September 2013; published 18 September 2013.

[1] As rivers transport water and sediment across Earth's surface, they radiate elastic and acoustic waves. We use seismic and infrasound observations during a controlled flood experiment (CFE) in the Grand Canyon to show that three types of fluvial processes can be monitored from outside the channel. First, bed-load transport under conditions of evolving bed mobility is identified as the dominant seismic source between 15 and 45 Hz. Two lower-frequency seismic bands also excited by the CFE exhibited greater power increases and are consistent with source processes related to fluid rather than sediment transport. The second fluvial seismic source is inferred to be fluid tractions on the rough riverbed, which drive the maximum seismic power increase at 0.73 Hz, but do not excite infrasound. Waves at the fluid-air interface are suggested as a third source, which generates a common 6–7 Hz peak in seismic and infrasound responses to the CFE. **Citation:** Schmandt, B., R. C. Aster, D. Scherler, V. C. Tsai, and K. Karlstrom (2013), Multiple fluvial processes detected by riverside seismic and infrasound monitoring of a controlled flood in the Grand Canyon, *Geophys. Res. Lett.*, *40*, 4858–4863, doi:10.1002/grl.50953.

1. Introduction

[2] Fluvial sediment transport and incision are fundamental landscape evolution processes that are effective at timescales relevant to land-use management and geological studies. Among the limitations in monitoring and modeling these processes is the difficulty of quantifying bed-load transport and the forces exerted on the riverbed. Existing methods for monitoring bed-load transport such as direct collection [e.g., *Leopold and Emmett*, 1977], tracking tracer particles [e.g., *Wilcock*, 1997], measuring vibrations in steel plates installed beneath riverbeds [e.g., *Turowski et al*., 2011], and monitoring of riverbed velocities [e.g., *Rennie et al*., 2002] provide valuable data, but often require considerable effort to monitor a single site. Additionally, there is concern that collection may interfere with the natural state of sediment transport, and that short sampling durations with any method can yield inaccurate estimates of longer-term transport rates [*Bunte and Abt*, 2005]. The potential benefits of new noninvasive, long-duration, and broadly applicable methods for monitoring riverbed processes have motivated research on the seismic signal emanating from rivers.

[3] There is growing observational and theoretical support for the concept of remotely monitoring bed-load transport by measuring ground vibrations outside the channel [e.g., *Govi et al*., 1993]. Using seismic observations that were primarily acquired to study Earth structure, *Burtin et al*. [2008] showed that 1–20 Hz noise levels were strongly correlated with discharge of the Trisuli River in Nepal. They further demonstrated that seismic power versus discharge exhibited seasonal hysteresis that is consistent with regional estimates of sediment transport rates [*Gabet et al*., 2008]. Similar hysteresis was also observed at 1–10 Hz at time scales of several days during storm events in the Cho-Shui River in Taiwan [*Hsu et al*., 2011]. Seismic observations of a small braided alpine stream [*Burtin et al*., 2011] suggest that gravel transport generates detectable seismic energy. These observations identify potential to develop methods for seismically monitoring bed-load flux, but rivers likely generate seismic energy through a diverse range of processes and their relative importance is poorly known.

[4] To better isolate fluvial seismic signals and link them to distinct processes, we collected data at the Colorado River during the November 2012 controlled flood experiment (CFE) in the Grand Canyon [e.g., *Topping et al*., 2010]. Our new seismic and infrasound observations take advantage of the predictable, large magnitude, and accurately known discharge variations. Additionally, we exploit the occurrence of a flash flood in a tributary canyon 3 months prior to the CFE, which locally increased the supply of weakly packed sediments. These circumstances in conjunction with 250 Hz seismic and infrasound sampling at only 38 m from the channel allow novel discrimination of multiple fluvial sources of seismic energy. Here we report on the characteristics of three distinct signals excited by the CFE. Based on their characteristics, we suggest that one of the signals dominantly results from bed-load transport and the other two dominantly result from fluid transport processes.

2. Field Site and Data

[5] The field site is in eastern Grand Canyon where the ephemeral Red Canyon tributary enters the Colorado River (see supporting information). Grand Canyon is a debris fan dominated channel with characteristic sequences of backwater

Additional supporting information may be found in the online version of this article.

[1]Department of Earth and Planetary Sciences, University of New Mexico, Albuquerque, New Mexico, USA.
[2]Department of Earth and Environmental Science, New Mexico Institute of Mining and Technology, Socorro, New Mexico, USA.
[3]Geosciences Department, Colorado State University, Fort Collins, Colorado, USA.
[4]Division of Geological and Planetary Science, California Institute of Technology, Pasadena, California, USA.
[5]Seismological Laboratory, California Institute of Technology, Pasadena, California, USA.

Corresponding author: B. Schmandt, Department of Earth and Planetary Sciences, University of New Mexico, Albuquerque, NM 87131, USA. (bschmandt@unm.edu)

0094-8276/13/10.1002/grl.50953

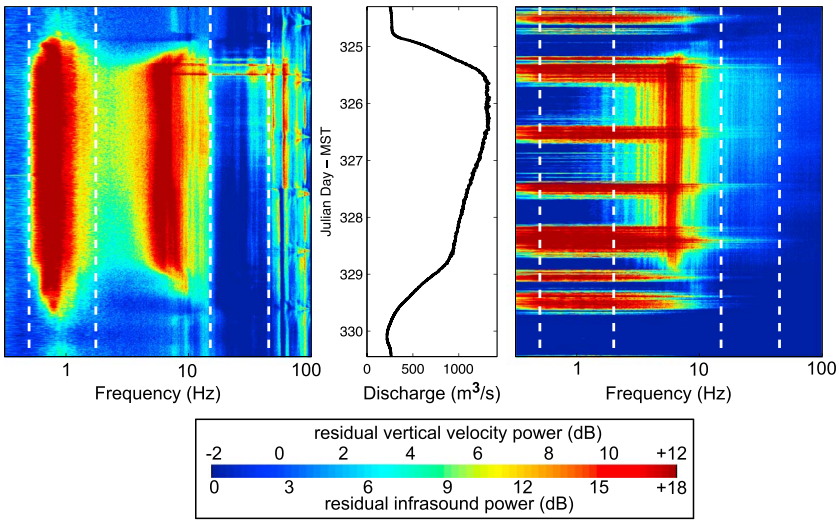

Figure 1. Vertical ground velocity and infrasound spectral response to the CFE. Figure 1 (left) shows the residual ground velocity spectrogram [dB rel. $(m/s)^2/Hz$], Figure 1 (middle) shows discharge, and Figure 1 (right) shows the residual infrasound spectrogram [dB rel. (Pa/s)/Hz]. The white dashed vertical lines label frequencies of 0.5, 2, 15, and 45 Hz. These delineate the frequency bands used in Figure 2. The lowest frequency peak in Figure 1 (left) is centered at 0.73 Hz, and the peak common to both the seismic and infrasound spectrograms is centered at 6.25 Hz.

pools upstream of tributary debris fans, coarse-grained debris fans, and eddies and associated sand and gravel bars downstream of debris fans [*Howard and Dolan*, 1981]. The Red Canyon confluence marks the beginning of Hance Rapid, which includes many 1–3 m standing water waves that span a downstream distance of about 150 m. Mean channel slope over a 1 km reach centered at Hance Rapid is 0.25%. Three months prior to the CFE, a flash flood in Red Canyon deposited poorly sorted sediment into the main channel at low discharge (<300 m^3/s) relative to peak CFE discharge of ~1300 m^3/s. Between the flash flood and CFE discharge never exceeded 550 m^3/s, and for 60 days prior to the CFE discharge was <280 m^3/s. This created a circumstance where the river's first interaction with naturally deposited sediments near the channel edge could be predictably recorded in addition to signals from elsewhere in the channel.

[6] The CFE hydrograph shows a factor of 5 increase in discharge over 1 day followed by sustained peak discharge of about 1300 m^3/s for 1 day and a more gradual 3 day decline back to the pre-CFE discharge (Figure 1). Peak CFE discharge is modest compared to the ~3500 m^3/s discharge of 10 year recurrence interval floods prior to dam installation [*Topping et al.*, 2010]. Peak stage increase above the pre-CFE level was typically 2–3 m near Hance Rapid and estimated by measuring the vertical distance between the post-CFE river surface and the highest vegetation disturbed by the CFE. Pre-CFE discharge is in the lower half of the 200–300 m^3/s range that is necessary to prevent sand accumulation in the Grand Canyon [*Topping et al.*, 2000], so pre-CFE transport of grains larger than sand is probably negligible. The nearest stream gages are located 27 km upstream and 16 km downstream of Hance Rapid and have a 15 min sampling period (www.gcmrc.gov). During the CFE, the largest tributary input downstream of Glen Canyon Dam was <6 m^3/s and no rainfall occurred. We linearly interpolate the upstream and downstream gage data to estimate the local discharge time series.

[7] Seismic and infrasound instruments were located 38 m from the channel edge at minimum discharge and about 32 m from the channel edge at peak CFE discharge. Three-component ground velocity was measured by an L-22 seismometer with a corner frequency of 2 Hz and flat response to >>100 Hz. Air pressure was measured by an infrasonic microphone with a corner frequency of 0.05 Hz and flat response to >>100 Hz [*Marcillo et al.*, 2012]. A 24-bit digitizer and a sampling rate of 250 Hz were used for both the seismic and infrasound recording. After deconvolution of the instrument response functions and application of an anti-aliasing filter, both types of data are reliable across the 0.3–100 Hz range presented here.

3. Spectral Analysis

[8] We focus on the river's response to the CFE in the frequency domain. Spectrograms were constructed using the multitaper method [*Thomson*, 1982] to estimate power spectral density in 2 min nonoverlapping windows. To minimize influence from spurious transients in the riverside environment, we examine the median spectrum across seven 2 min windows at a time. Vertical and mean horizontal spectra are analyzed. The mean of the two horizontal components is used because source processes of interest are distributed at uncertain locations in the river channel. To examine the spectral response to changes in discharge, we calculated the median spectra during times of minimal discharge (200–240 m^3/s) prior to the CFE and subtract them from the raw spectrograms to yield residual spectrograms (Figure 1; see supporting information).

4. Seismic and Infrasonic Response to the CFE

[9] Residual ground velocity power increased with discharge in multiple frequency bands during the CFE (Figure 1). The lowest frequency band excited by the CFE is 0.5–2 Hz, with a maximum increase of 17 dB at 0.73 Hz.

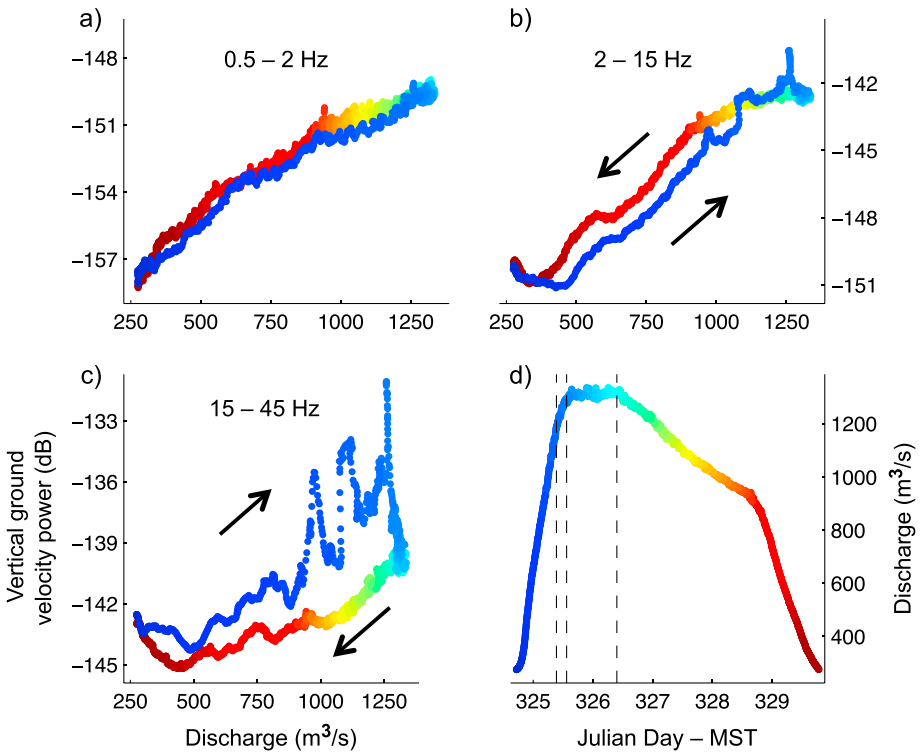

Figure 2. Frequency-dependent hysteresis. (a) Vertical ground velocity power [dB rel. $(m/s)^2/Hz$] from 0.5 to 2 Hz versus discharge. (b) Vertical power from 2 to 15 Hz versus discharge exhibits weak counter-clockwise hysteresis for discharge between 375 and 1050 m^3/s. (c) Power from 15 to 45 Hz shows strong clockwise hysteresis with variably greater power (up to 9 dB) during the rising limb of the CFE compared to the plateau or lagging limb. (d) The CFE hydrograph is color-coded by time with the same scale used in Figures 2a–2c. Vertical dashed lines bound the "rising" and "plateau" time segments used in Figure 3.

A second local maximum of 14 dB increase occurs at 6.25 Hz. Frequencies from about 10–45 Hz show bursts of elevated power during near the end of the CFE's rising limb. However, power between about 15–45 Hz returns to near pre-CFE levels during the descending limb while discharge is still about 1000 m^3/s. Thus, two peaks in the residual seismic spectrum remain prominent throughout the duration of the CFE, while frequencies between about 15–45 Hz are strongly excited during the rising limb but not the descending limb.

[10] Residual infrasound power also increases with discharge and has a maximum between 6 and 7 Hz that is maintained during the rising and descending limbs. Additional peaks in the infrasound spectrogram appear as horizontal bands at <10 Hz that have a quasi-diurnal recurrence, vary in duration from 2 to 12 h, and are not correlated with variations in discharge. These features are attributed to wind because it is a common source of $\leq$10 Hz infrasound noise [e.g., *Hedlin and Raspet*, 2003], and we observed one of these episodes during fieldwork on a windy day.

[11] The distinct seismic bands excited by the CFE show contrasting temporal variations (Figure 2). Hysteresis between seismic power and discharge is clearly exhibited by the 15–45 Hz band, but is relatively subtle or absent in the two lower-frequency bands. If this frequency band is extended to as low as 10 Hz or as high as 60 Hz, observation of hysteresis and its magnitude remains similar. In addition to the clockwise pattern of hysteresis, the 15–45 Hz band has three episodes with 4–5 dB power increases for durations of about 30–70 min during the latter half of the CFE's rising limb. Between these episodes, power remains 1.5–3 dB higher than at the same discharge during the descending limb. The final high-power episode is truncated at the time of the transition from the rising limb to constant peak discharge, when seismic power drops by 9 dB (Figure 2c). Episodic seismic power increases and hysteresis are small or absent in the two lower-frequency bands (Figure 2). The lowest frequency band excited by the CFE, 0.5–2 Hz, shows smoothly increasing power with discharge, steady power during the plateau at peak discharge, and the rising and descending limbs are consistent within 1 dB. The 2–15 Hz band also shows steady power during the plateau at peak discharge, but weak counter-clockwise hysteresis between 375–1050 m^3/s. At these intermediate discharge levels, power during the descending limb is greater by about 1 dB. The 2–15 Hz band also shows power increases at the times of the episodic bursts of 15–45 Hz power, although they are relatively subtle indicating that the source of these bursts overlaps the boundary at 15 Hz.

[12] To isolate the part of the spectrum that shows the greatest power variations despite nearly constant discharge, we compare the median spectrum during the last 200 min of the rising limb to the median spectrum during the plateau at peak discharge (Figure 3). Discharge during these two time segments differs by only 5%. Power during the rising limb segment is greater than during the plateau segment from about 10–60 Hz with greatest difference between 15–45 Hz (Figure 3c). A similar difference is observed for the

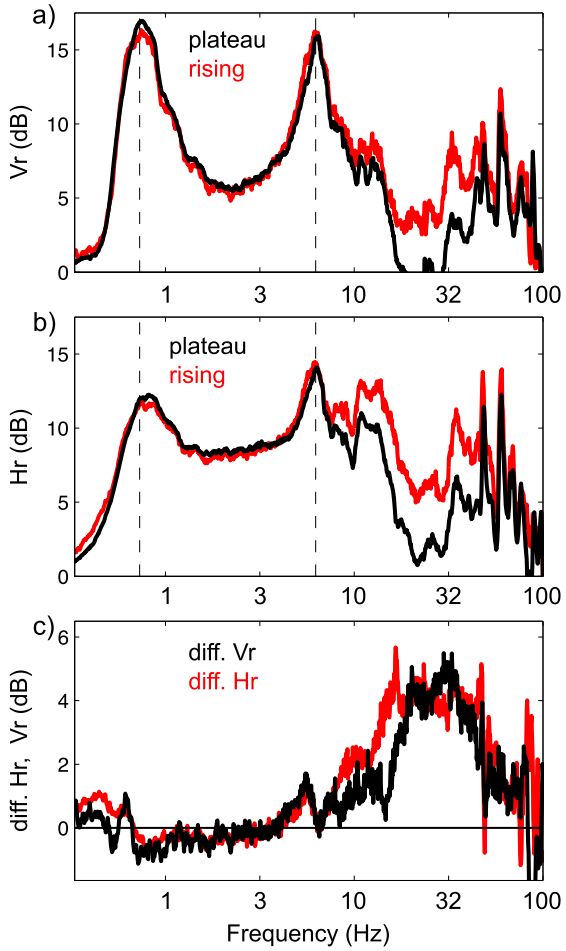

Figure 3. Spectra from the "rising" and "plateau" phases of the CFE. (a) The median vertical component residual spectra (Vr) during the last 200 min of the "rising" and "plateau" phases of the hydrograph are shown in red and black, respectively. (b) Analogous to Figure 3a, but the median horizontal residual spectrum (Hr) is shown during the two hydrograph phases. Two data gaps, comprising <10% of the plateau phase, were omitted from estimation of both Vr and Hr in this figure (see supporting information). (c) The difference between Hr and Vr during the rising and plateau phases is shown in red and black, respectively. Dashed vertical lines label frequencies of 0.5, 2, 15, and 45 Hz.

horizontal spectra. The two lower-frequency maxima are nearly constant for the rising and plateau time periods. Additionally, the lower frequency peaks are stronger in the vertical compared to the horizontal spectrum, with a difference of up to 4.5 dB in the lowest band.

4.1. Fluvial Sources of Seismic Energy

[13] Based on the contrasting characteristics of the different frequency bands excited by the CFE, we interpret that distinct fluvial processes are responsible. Specifically, we suggest that the following three source processes can be distinguished by combined seismic and infrasound monitoring at this site: bed-load transport, fluid tractions exerted on the rough riverbed, and fluid-air interactions such as breaking waves.

4.2. The Seismic Signal of Bed-Load Transport

[14] We consider the 15–45 Hz power variations to be dominantly driven by bed-load transport, although a contribution from bed-load likely extends to somewhat higher and lower frequencies (Figure 3c). This attribution is suggested by strong clockwise hysteresis, including 1–9 dB power differences for equivalent discharge and three episodes with 4–5 dB power increases for about 30–70 min during smoothly rising discharge. These temporal fluctuations in power are inconsistent with generation by smoothly varying fluid discharge. In contrast, bed-load transport has long observed to be temporally heterogeneous [e.g., *Leopold and Emmett*, 1977], including episodic pulses of increased flux [e.g., *Reid et al*., 1985] and both clockwise and counter-clockwise hysteresis in bed-load transport versus discharge [e.g., *Hsu et al*., 2011]. Recent flood simulations in a flume with heterogeneous grain sizes consistently exhibited clockwise hysteresis of bed-load flux versus discharge for a variety of hydrograph shapes [*Mao*, 2012].

[15] Power in the 15–45 Hz band began to increase consistently when discharge rose above about 550 m^3/s, which is the maximum discharge that occurred between the flash flood and the CFE. Thus, the first interaction between the main channel flow and poorly packed sediments from Red Canyon is likely the dominant bed-load transport activity at the study site. Reworking of the flash flood deposits by the main channel flow during the CFE's rising limb may have resulted in tighter packing and preferential transport of fine grains [e.g., *Mao et al*., 2011] or changes in the friction angle without changing the surface grain-size distribution [e.g., *Kirchner et al*., 1990]. Either could increase the critical shear stress, such that steady peak discharge resulted in lower bed-load transport rates and 15–45 Hz seismic power than during the latter half of the rising limb. Post-CFE observations found that a sediment bar composed of gravel and larger clasts remained at the mouth of Red Canyon, supporting that variation in critical shear stress rather than exhaustion of sediment caused the 9 dB drop in seismic power at the end of the rising limb.

[16] A simple estimate of relative variations in bed-load flux can be made following the assumptions of *Tsai et al*. [2012]. They noted that variations in vertical seismic power scale linearly with bed-load mass flux if transport occurs by saltation of spherical grains on a flat elastic riverbed, and the spatial distribution of saltating grains remains constant. In this model, the episodes with 4–5 dB power increases would correspond to transient increases in bed-load flux by a factor of 2.5–3.2, and the 9 dB drop in power at the end of the rising limb would correspond to an abrupt eightfold decrease in bed-load flux. However, assumptions of the *Tsai et al*. [2012] model such as vertical saltation, spherical grains and a flat bed, and a constant spatial distribution of bed-load transport may not be accurate, so the estimates above are highly uncertain.

[17] Isolation of the seismic power spectrum dominated by bed-load transport (Figure 3c) allows comparison with the vertical spectrum predicted by the *Tsai et al*. [2012] model. Source-receiver distance is the primary control on the frequency content in the model. With an attenuation factor or Q of 8 and distance of 35 m from the river, the model is consistent with the ~30 Hz peak we observe. The requirement of a Q of 8 to match the spectral peak is plausible, but perhaps too high as Q = 9 was found at <150 m depth in highly weathered granite [*Aster and Shearer*, 1991], and our sensor

was deployed on alluvium. It is also possible that grain-size distribution affects the seismic power spectrum more strongly than predicted by *Tsai et al*. [2012]. Experimental results from vertically dropping rocks show decreasing frequency with increasing grain size, and also a broader frequency response for rolling rather than vertical impacts [*Huang et al*., 2007].

[18] In theory, the dominant elastic wave type generated by a vertical force at the riverbed would be Rayleigh waves [e.g., *Tsai et al*., 2012], such that mean power of the two horizontal components would be less than the vertical power. At the site near Hance Rapid, we find approximately equal power in the vertical and horizontal spectra in the inferred bed-load transport frequency band (Figure 3c). This suggests that factors such as bed roughness and rolling or sliding mechanisms are probably important, as they would enhance the generation of horizontally polarized Love waves.

4.3. Two Seismic Sources From Fluid Processes

[19] At the study site, bed-load transport is not the dominant source of seismic power during the CFE. Two lower-frequency seismic bands exhibit greater power increases than in the 15–45 Hz band we infer to be dominated by bed-load transport. Power in both the 0.5–2 Hz and 2–15 Hz bands varies more smoothly with discharge and remains steady during peak discharge. A major difference between these two signal bands is that the lower band, which contains the greatest seismic power increase, is not excited in the infrasound spectrum and the higher seismic band closely corresponds with the maximal infrasound response to the CFE.

[20] We attribute the increased power in the 0.5–2 Hz band primarily to turbulent fluid flow that exerts pressure on the riverbed, which is probably enhanced by flow over boulders. In Grand Canyon rapids, such as Hance Rapid, the riverbed is generally covered by boulders and talus that were only partially mobilized by pre-dam floods greater than ~3000 m^3/s [*Howard and Dolan*, 1981] so a continuously active layer of bed sediments is unlikely. Smooth power variations with discharge and lack of hysteresis are consistent with a fluid flow source. Lack of an infrasound response in this frequency band further suggests a source process limited to the fluid-solid interface. The 0.73 Hz maximum is 4.5 dB stronger in the vertical than horizontal spectrum indicating that vertical tractions dominate over shear tractions at the source (Figure 3). We suggest that fluid flow over the rough riverbed in Hance Rapid is the source of dominantly vertical tractions whose magnitude varies smoothly with discharge.

[21] Power in the 2–15 Hz band is primarily attributed to fluid-air interactions in Hance Rapid. There appears to be overlap between this signal and the bed-load signal between about 6–15 Hz, but steady power near the 6.25 Hz peak throughout the time of near-maximal discharge suggests that fluid transport creates the majority of the seismic power below ~15 Hz (Figure 3). Coincidence of the local maxima of residual seismic and infrasound power is the basis for our interpretation that fluid-air interactions are the dominant source. Seismic power in the 2–15 Hz band exhibits counter-clockwise hysteresis restricted to discharge values of 375–1000 m^3/s and with ~1 dB greater power on the descending limb. If waves at the fluid-air interface are primarily responsible for power in this band, the difference at intermediate discharge levels could represent a modest change in the water wave pattern owing to bed-load movement during peak discharge.

5. Conclusions

[22] We have shown that the seismic response to the CFE is peaked in three distinct frequency bands that exhibit contrasting temporal evolutions during the CFE. Sources related to fluid transport are identified by their lack of sporadic power fluctuations and subtle or absent hysteresis. Sources of this type comprise the majority of the seismic power increase during the CFE and produce maxima in two different seismic bands. The lower band is absent in the infrasound spectrum and is consequently attributed to fluid tractions on the riverbed, while the higher band coincides with the maximal infrasound response and is attributed to waves at the fluid-air surface. Similar to prior studies, a bed-load contribution is indentified by clockwise hysteresis between seismic power and discharge. In addition, we detect transient increases in bed-load transport rate during the rising limb and use differential spectra between the end of the rising limb and plateau at peak discharge to isolate the spectrum of the bed-load signal. Nearly equal power of the bed-load signal in the vertical and mean horizontal spectra indicates that Love and Rayleigh waves should be considered in methods to seismically monitor bed-load flux.

[23] **Acknowledgments.** We thank M. Hahn and R. Newton from the National Park Service, and J. Schmidt, C. Fritzinger, N. Voichick, and R. Tusso from the Grand Canyon Monitoring and Research Center for making it possible to use this exceptional science opportunity. The IRIS PASSCAL Instrument Center, and particularly P. Miller and G. Slad are thanked for instrument and data handling support. E. Aster assisted with fieldwork. Mike Lamb provided informal feedback. Two anonymous reviewers helped improve the manuscript. B.S. acknowledges Caltech for time to conduct fieldwork and support for this research from the University of New Mexico.

[24] The Editor thanks two anonymous reviewers for their assistance in evaluating this paper.

References

Aster, R. C., and P. M. Shearer (1991), High-frequency borehole seismograms recorded in the San Jacinto Fault Zone, Southern California, Part 2. Attenuation and site effects, *Bull. Seismol. Soc. Am.*, *81*, 1081–1100.

Bunte, K., and S. R. Abt (2005), Effect of sampling time on measured gravel bed load transport rates in a coarse bedded stream, *Water Resour. Res.*, *41*, W11405, doi:10.1029/2004WR003880.

Burtin, A., L. Bollinger, J. Vergne, R. Cattin, and J. L. Nabelek (2008), Spectral analysis of seismic noise induced by rivers: A new tool to monitor spatiotemporal changes in stream hydrodynamics, *J. Geophys. Res.*, *113*, B05301, doi:10.1029/2007JB005034.

Burtin, A., R. Cattin, L. Bollinger, J. Vergne, P. Steer, A. Robert, N. Findling , and C. Tiberi (2011), Towards the hydrologic and bed load monitoring from high-frequency seismic noise in a braided river: The "torrent de St Pierre", French Alps, *J. Hydrol.*, *408*(1–2), 43–53, doi:10.1016/j.jhydrol.2011.07.014.

Gabet, E. J., D. W. Burbank, B. Pratt-Sitaula, J. Putkonen, and B. Bookhagen (2008), Modern erosion rates in the high Himalayas of Nepal, *Earth Planet. Sci. Lett.*, *267*, 482–494.

Govi, M., F. Maraga, and F. Moia (1993), Seismic detectors for continuous bed-load monitoring in a gravel stream, *Hydrol. Sci. J.*, *38*(2), 123–132, doi:10.1080/02626669309492650.

Hedlin, M. A. H., and R. Raspet (2003), Infrasonic wind noise reduction by barriers and spatial filters, *J. Acoust. Soc. Am.*, *114*, 1379–1386.

Howard, A., and R. Dolan (1981), Geomorphology of the Colorado River in the Grand Canyon, *J. Geol.*, *89*(3), 269–298.

Hsu, L., N. J. Finnegan, and E. E. Brodsky (2011), A seismic signature of river bed-load transport during storm events, *Geophys. Res. Lett.*, *38*, L13407, doi:10.1029/2011GL047759.

Huang, C.-J., H.-Y. Yin, C.-Y. Chen, C.-H. Yeh, and C.-L. Wang (2007), Ground vibrations produced by rock motions and debris flows, *J. Geophys. Res.*, *112*, F02014, doi:10.1029/2005JF000437.

Kirchner, J. W., W. E. Dietrich, F. Iseya, and H. Ikeda (1990), The variability of critical shear stress, friction angle, and grain protrusion in water worked sediments, *Sedimentology*, *37*, 647–672, doi:10.1111/j.1365-3091.1990.tb00627.x.

Leopold, L. B., and W. W. Emmett (1977), 1976 bedload measurements, East Fork River, Wyoming, *Proc. Natl. Acad. Sci. U. S. A.*, *74*(7), 2644–2648, doi:10.1073/pnas.74.7.2644.

Mao, L. (2012), The effect of hydrographs on bed load transport and bed sediment spatial arrangement, *J. Geophys. Res.*, *117*, F03024, doi:10.1029/2012JF002428.

Mao, L., J. R. Cooper, and L. E. Frostick (2011), Grain size and topographical differences between static and mobile armor layers, *Earth Surf. Processes Landforms*, *36*, 1321–1334, doi:10.1002/esp.2156.

Marcillo, O., J. B. Johnson, and D. Hart (2012), Implementation, characterization, and evaluation of an inexpensive low-power low-noise infrasound sensor based on a micromachined differential pressure transducer and a mechanical filter, *J. Atmos. Oceanic Technol.*, *29*, 1275–1284, doi:10.1175/JTECH-D-11-00101.1.

Reid, I., L. E. Frostick, and J. T. Layman (1985), The incidence and nature of bed-load transport during flood flows in coarse grained alluvial channels, *Earth Surf. Processes Landforms*, *10*(1), 33–44, doi:10.1002/esp.3290100107.

Rennie, C. D., R. G. Millar, and M. A. Church (2002), Measurement of bed load velocity using an acoustic Doppler current profiler, *J. Hydraul. Eng.*, *128*, 473–483.

Thomson, D. J. (1982), Spectrum estimation and harmonic analysis, *Proc. IEEE*, *70*(9), 1055–1096.

Topping, D. J., D. M. Rubin, and L. E. J. Vierra (2000), Colorado River sediment transport 1. Natural sediment supply limitation and the influence of Glen Canyon Dam, *Water Resour. Res.*, *36*(2), 515–542.

Topping, D. J., D. M. Rubin, P. E. Grams, R. E. Griffiths, T. A. Sabol, N. Voichick, R. B. Tusso, K. M. Vanaman, and R. R. McDonald (2010), Sediment transport during three controlled-flood experiments on the Colorado River downstream from Glen Canyon Dam, with implications for eddy-sandbar deposition in Grand Canyon National Park: U.S. Geological Survey Open-File Report 2010–1128, 111 p.

Tsai, V. C., B. Minchew, M. P. Lamb, and J.-P. Ampuero (2012), A physical model for seismic noise generation from sediment transport in rivers, *Geophys. Res. Lett.*, *39*, L02404, doi:10.1029/2011gl050255.

Turowski, J. M., A. Badoux, and D. Rickenmann (2011), Start and end of bed-load transport in gravel bed streams, *Geophys. Res. Lett.*, *38*, L04401, doi:10.1029/2010GL046558.

Wilcock, P. R. (1997), Entrainment, displacement and transport of tracer gravels, *Earth Surf. Processes Landforms*, *22*, 1125–1138.